Nucleation and Growth of Perfluoropentacene on Self-Assembled Monolayers: Significant Changes in Island Density and Shape with Surface Termination

Tushar V. Desai,[†] Arthur R. Woll,[‡] Frank Schreiber,[§] and James R. Engstrom*,[†]

School of Chemical and Biomolecular Engineering and Cornell High Energy Synchrotron Source, Cornell University, Ithaca, New York 14853, United States, and Institut für Angewandte Physik, Universität Tübingen, 72076 Tübingen, Germany

We have examined the nucleation and growth of perfluoropentacene (PFP) on SiO_2 and on a variety of surfaces possessing different terminating self-assembled-monolayers (SAMs) using in situ synchrotron X-ray scattering and ex situ atomic force microscopy. The SAMs ranged from very low surface energy hydrophobic surfaces (perfluorooctyltrichlorosilane) to higher surface energy hydrophilic surfaces (3-methacryloxypropyltrichlorosilane). From real time X-ray scattering, we find that the growth of PFP, while crystalline, becomes very three-dimensional after completion of the first 1−2 monolayers, independent of the substrate surface termination. Concerning growth in the submonolayer regime, we find that nucleation is homogeneous and that the absolute density of islands depends strongly on the surface termination, while the relative change of the island density with increasing growth rate is essentially independent of the underlying SAM. From the latter, we find that a critical island size of ∼2−3 molecules can describe all of the data. On the other hand, the dependence of the island density on termination implicates a significant change in the diffusivity of PFP with the identity of the SAM. The shape of the islands also depends on the surface termination but somewhat unexpectedly—the islands are most compact and faceted on surfaces where the diffusivity of isolated PFP molecules is the smallest. This result highlights the difference in transport mechanisms concerning diffusion across the substrate and that around the periphery of an island in molecular systems. Finally, on all surfaces, the films formed in the multilayer regime are similar and are described by rough, highly anisotropic features, perhaps dominated by a single low index face.

I. Introduction

The study of complex conjugated molecules for applications in organic thin film electronics and photonics has received much attention because of their ability to form highly ordered thin films with excellent electrical properties.[1−3] Studies have shown that the interface between the organic semiconducting layer and the dielectric is critical to charge transport and that the majority of charge carriers are generated in the first few monolayers (MLs) of the organic layer.[4−7] Several studies have also shown that the deposition of organic semiconductors on low energy surfaces such as self-assembled monolayers (SAMs) significantly improves the electrical properties of the organic thin film transistor (OTFT).[8−12] The exact reasons as to why this improvement is observed are still a matter of debate, however. Clearly, the development of a better understanding of the effects of SAMs on the nucleation and the initial stages of growth of organic semiconductors, particularly in the submonolayer regime, will greatly aid in resolving these issues.

There have been a number of investigations of the nucleation of pentacene on clean, unmodified, silicon dioxide (SiO_2), and the consensus is that the nucleation is homogeneous with the size of the critical cluster being ∼2−6 molecules.[13−15] The study of the effects of SAMs on the nucleation of organic semiconductors, pentacene or otherwise, has proven to be more challenging. A major obstacle to be overcome in these systems is that pentacene and other organic thin films undergo significant, and sometimes rapid, postgrowth reorganization and dewetting when deposited on low energy surfaces.[16,17] One system, due to its low intrinsic surface energy, that might not be expected to dewet low energy surfaces of SAMs is the *n*-type organic semiconductor perfluoropentacene (PFP). Thus, this property of PFP can be exploited to examine in detail effects occurring in the submonolayer nucleation and growth of organic small molecule thin films on surfaces terminated with SAMs.

Here, we report on the effects of SAMs on the nucleation and growth of PFP using a combination of both in situ and ex situ surface sensitive probes. Concerning the SAMs, we consider four layers that differ in terms of their size (thickness) and chemical nature: octyltrichlorosilane (OTS), $(Cl)_3Si-(CH_2)_7-CH_3$, perfluorooctyltrichlorosilane (FOTS), $(Cl)_3Si-(CH_2)_2-(CF_2)_5-CF_3$, 3-methacryloxypropyltrichlorosilane (MAOPTS), $(Cl)_3Si-(CH_2)_3-O-(C=O)(C(CH_3)=CH_2)$, and hexamethyldisilazane (HMDS), $HN(Si(CH_3)_3)_2$. The first three of these hydrolyze to form $-Si(-O-)_3$ linkages to the SiO_2 surface of the substrates, whereas HMDS decomposes and releases $-Si(CH_3)_3$ fragments, which then bind to the surface. For comparison, we also consider unmodified SiO_2. In terms of surface energies, the SAMs follow the order (high-to-low): unmodified SiO_2, MAOPTS, HMDS, OTS, and FOTS. We deposit thin films of PFP in ultrahigh vacuum (UHV) using a collimated supersonic molecular beam[13,18,19] and make use of ex situ atomic force microscopy (AFM) to probe the thin film morphology, focusing on the submonolayer regime. We also

* To whom correspondence should be addressed. Tel: 607-255-9934. Fax: 607-255-9166. E-mail: jre7@cornell.edu.
[†] School of Chemical and Biomolecular Engineering, Cornell University.
[‡] Cornell High Energy Synchrotron Source, Cornell University.
[§] Universität Tübingen.

Nucleation and Growth of Perfluoropentacene on SAMs

J. Phys. Chem. C, Vol. 114, No. 47, 2010 **20121**

employ in situ real-time synchrotron X-ray scattering measurements at the "anti-Bragg" configuration[20] to directly probe the filling of each successive molecular layer of PFP. We will find below that the nature of the SAM affects significantly both the density and the shape of the islands formed at submonolayer coverages.

II. Experimental Procedures

The experiments were carried out in the G3 station of the Cornell High Energy Synchrotron Source in a custom-designed UHV system, described elsewhere, fitted with Be windows.[18,19] Briefly, the system consists of four separately pumped chambers: a main scattering chamber, a source and antechamber, which act to produce the supersonic beam, and a fast entry load-lock. All chambers are pumped by high-throughput turbomolecular pumps. The base pressure of the chamber was typically $\sim 4 \times 10^{-9}$ Torr, and samples were loaded via the load-lock chamber, which was evacuated to $\sim 10^{-7}$ Torr prior to sample transfer into the main chamber.

Substrates were Si(100) wafers (Wacker-Siltronic, p type, 100 mm diameter, 500−550 μm thick, 38−63 Ω cm) subject to a SC-1 clean, 15 s HF dip and a SC-2 clean followed by growth of $\sim$300 nm thick SiO_2 films by wet thermal oxidation at 1100 °C. Next, these wafers were cleaned and degreased by sonication for 15 min in anhydrous $CHCl_3$ solution (99%+), sonicated in deionized (DI) water for 15 min, washed with DI water, dried with N_2, and exposed to UV ozone for 15 min. These processes provided a clean and reproducible hydrophilic surface. Finally, the SAMs were deposited using established procedures.[21] Briefly, the FOTS and MAOPTS layers were deposited from the vapor phase using an MVD-100 system, while the HMDS was deposited from the vapor phase using a YES LP-III Vapor Prime Oven. OTS was deposited from the solution phase in a N_2-purged glovebox.

Supersonic molecular beams of PFP were generated by passing He (99.999% Air Gas Inc.) as a carrier gas over an in situ temperature-controlled evaporator located upstream of the 150 μm diameter nozzle in the source chamber. The flow of He was set by a mass flow controller. The beam passes through a 1.5 mm diameter skimmer, into the antechamber, and through an aperture to produce a well-defined beam spot on the substrate (4 × 15 mm²) at normal incidence. The kinetic energy of the beam was measured using time-of-flight mass spectrometric techniques[18] and kept constant for all experiments at $E_i = 4.6$ eV. For all experiments described here, the substrate temperature during growth was $T_s = 40$ °C, and in all cases, the beam was incident normal to the substrate surface and could be blocked using a shutter in the antechamber. Multiple experiments could be carried out on the same substrate, which is made possible by translating the substrate perpendicular to the supersonic molecular beam and because of the high beam-to-background flux ratio. Following deposition, AFM was conducted ex situ in tapping mode using a Digital Instruments 3100 Dimension microscope.

The SiO_2 substrates modified with FOTS, OTS, HMDS, and MAOPTS, were characterized by contact angle and X-ray reflectivity (XRR). First, contact angles were measured in two solvents (water and formamide). Next, using the Young−Dupre equation,[22] we calculated the surface energy of FOTS, OTS, HMDS, and MAOPTS and found values of 11.1, 16.7, 32.7, and 40.1 mJ m^{-2}, respectively. In comparison, the surface energy of clean, unmodified SiO_2 has been reported to lie between 50 and 60 mJ m^{-2}.[23,24] Fits to the XRR data (not shown) were performed with the Parratt32 software package[25] (based on the
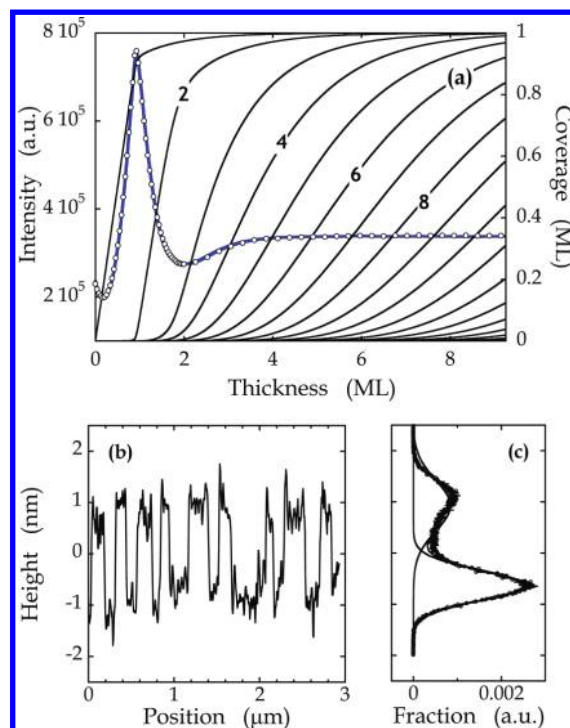

Figure 1. (a) X-ray intensity at the anti-Bragg condition as a function of exposure to the molecular beam ($E_i = 4.6$ eV) for thin films of PFP deposited on a SiO_2 surface terminated with HMDS. The substrate temperature, $T_s = 40$ °C, and the rate of growth was 0.0103 ML s^{-1}. The thick solid blue line (left ordinate) indicates a fit of the data to a model, and thin solid black curves (right ordinate) represent predicted coverages of the individual layers. Representative (b) line scan and (c) surface height histogram obtained from AFM of a submonolayer PFP thin film (0.36 ML) grown on HMDS.

Parratt formalism[26]), from which we obtain the thickness of the organic layers and the mean electron density. Knowledge of the molecular weight of the SAM molecules permits us to estimate the two-dimensional (2D) surface concentration of the SAMs. For all four SAMs, we found values in the range of $2-3 \times 10^{14}$ molecules cm^{-2}, similar to values found using XRR and X-ray photoelectron spectroscopy[27] for these same SAMs.

III. Results and Discussion

We first consider measurements of film growth using in situ real time synchrotron X-ray scattering. Here, growth of PFP was monitored using 9.82 keV X-rays incident at an angle of 1.15° (with respect to the substrate surface) with a flux of $\sim 10^{13}$ photons s^{-1} (unattenuated value, the beam was attenuated for all experiments) incident to the sample through a Be window with energy resolution of 1%, which was dictated by the use of a multilayer monochromator. An avalanche photodiode (Oxford Danfysik, Oxford, United Kingdom) was used to measure the scattered X-ray intensity. First, we consider X-ray reflectivity measurements at the so-called "anti-Bragg" condition (00½; $q_z = q_{Bragg}/2 = 0.40/2$ Å^{-1}), which is an effective monitor of the nature of growth, that is, layer-by-layer (LbL) vs three-dimensional (3D) islanded growth.[19,28,29]

In Figure 1a, we plot the scattered intensity measured in situ and in real time for the growth of PFP on HMDS at $E_i = 4.6$ eV. As may be seen, for growth on this surface, we observe a single sharp, cusplike peak, which coincides with completion of the first ML, but the anticipated second (small, similar to the zero-coverage intensity), third (large, similar to the first peak), and other subsequent maxima are almost completely

obscured. Beyond the deposition of four MLs, the intensity remains constant. This suggests that growth becomes 3D quickly after completion of the first 1–2 MLs. The intensity oscillation can be fit using a modified version[30] of the mean-field, rate equation model of growth first proposed by Cohen and co-workers.[31] The fit to the intensity is indicated by the solid blue line, and we see that the fit to the experimental data is excellent. In Figure 1a, we also show the coverage (occupancy) of each layer with solid black lines that are predicted by the fit to the intensity oscillations. After a total growth of two MLs, the second layer is ~81% full, whereas after four MLs, the fourth layer is only ~59% full. These results indicate that PFP grows in an LbL mode for approximately two MLs before significant roughening begins to occur. Indeed, we observe essentially identical behavior concerning the intensity oscillations at the anti-Bragg condition for growth on all four SAMs examined here, on unmodified SiO$_2$, and for incident kinetic energies over the range of $E_i = 4.6$–16.4 eV. We note that this behavior has also been observed for growth of PFP from a thermal effusion source on a thin layer of native SiO$_2$.[32,33]

In Figure 1b, we display a representative line profile obtained from ex situ AFM of the islands formed after deposition of ~0.36 ML of PFP on a HMDS-terminated surface at a growth rate of 0.0056 ML s^{-1}. In Figure 1c, we display a histogram of surface heights calculated from the entire AF micrograph. The line profile and histogram indicate that the islands of PFP on HMDS are single ML-tall islands with an average height of ~1.61 ± 0.04 nm. This height is consistent with ex situ specular XRR measurements of ~10 ML thick films of PFP deposited on a variety of surfaces (including clean, unmodified SiO$_2$) where a unit cell height of $d_{001} = 1.57 \pm 0.02$ nm was found.[32–35] We note that following deposition, AF micrographs of submonolayer growth of PFP reveal single ML tall high islands on all of the surfaces that we have investigated. This is also the case where the submonolayer films have experienced extended aging, postdeposition, for time periods in vacuum for ≥ 2 h (as opposed to <2 min more typically here) and in air for several months. This indicates that PFP does not reorganize or "dewet" on these surfaces unlike other conjugated organic semiconductors such as pentacene[16] and diindenoperylene (DIP), where such behavior has been observed on surfaces terminated with both HMDS and FOTS layers. The relative stability of the submonolayer islands of PFP is of course essential to the main objectives of this work.

In Figure 2a–d, we display AF micrographs of PFP deposited on HMDS at a series of growth rates (GRs), increasing in sequence from 0.0024 to 0.018 ML s^{-1}, with all other parameters (e.g., E_i and T_s) fixed. The growth rate of PFP has been tuned by varying the temperature of the in situ evaporator. On this surface, the shapes of the islands at all growth rates are polygons and anisotropic, with an aspect ratio ~2–3. At this stage of growth, the islands are also mostly isolated from each other, such that we can use these images to calculate the maximum island density. As the field of view is the same in all cases (3×3 μm^2), we see by inspection that the island density of PFP increases with increasing GR. The scaling of the island density with GR in this way is exactly as expected from classical nucleation theory for homogeneous nucleation,[36–38] which states that the maximum island density, N_x, for 2D islands and complete condensation (adsorption is irreversible) is given by the following expression:

$$N_x = \eta(\theta, i^*)(\mathrm{GR}/D)^{i^*/(i^*+2)} \exp[E_{i^*}/(i^*+2)k_B T_s]$$
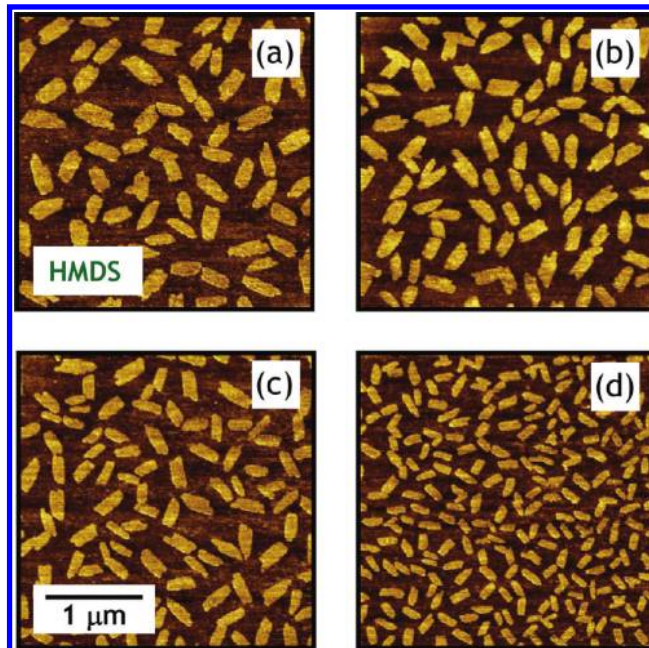
$$(1)$$

Figure 2. Atomic force micrographs, 3×3 μm^2, of submonolayer thin films of PFP grown on a SiO$_2$ surface terminated with HMDS at rates of (a) 0.00240, (b) 0.00424, (c) 0.00561, and (d) 0.0180 ML s^{-1}. In all cases, the incident kinetic energy was $E_i = 4.6$ eV, and the substrate temperature was $T_s = 40$ °C.

where D is the tracer diffusivity of the molecule, i^* is the critical cluster size, E_{i^*} is the binding energy of the critical cluster, and k_B is the Boltzmann constant. The critical cluster size is defined as the largest unstable cluster, such that a cluster with $i^* + 1$ molecules is more likely to grow than to decay. The dimensionless prefactor $\eta(\theta, i^*)$ is nearly a constant—only weakly dependent on i^* and coverage, θ.[37] Thus, one straightforward measurement of the critical cluster size is to quantify how the maximum island density varies with GR[36–39] (cf. Figure 2a–d).

In Figure 3, we display the maximum island density as a function of GR for PFP on the five surfaces that we consider here. The maximum island densities of PFP were measured at submonolayer coverages ($\theta < 0.43$ ML) before island coalescence took place using 10×10 μm^2 (3×3 μm^2 for PFP on FOTS) AF micrographs. As may be seen in the figure, the maximum island density of PFP increases with increasing GR on all surfaces, and the data are described very well by a power law in all cases. This would seem to argue against any interpretation involving defects in the SAMs playing a significant or dominant role in the nucleation. Thus, it seems that regardless of the nature of the underlying interfacial layer, PFP exhibits homogeneous nucleation on all surfaces. The critical cluster size of PFP can be determined from the power law fit to the data, and our results are displayed in the inset of Figure 3. Here, in a fit to the data, we have considered explicitly the uncertainty in each value for the density of the islands ($N^{1/2}$, where N is the direct count of the islands in the image). As may be seen, we find similar values for the power law exponents, and they span the range of $i^* = 2.4$–3.7. The results on HMDS, OTS, unmodified SiO$_2$, and MAOPTS are all very similar, and the mean value for these four surfaces is given by $i^* = 2.66 \pm 0.36$. FOTS is somewhat of an outlier from these results, albeit the uncertainty is greater, and we find $i^* = 3.68 \pm 0.61$. Thus, possibly except for the case of FOTS, the interactions between the substrate surface and the PFP molecules do not significantly affect the critical cluster size of PFP.
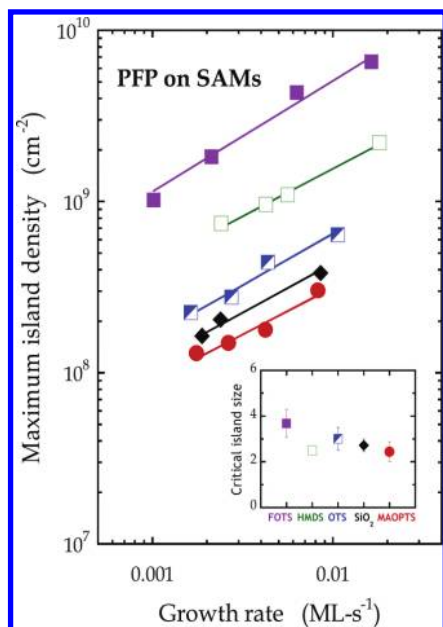
Nucleation and Growth of Perfluoropentacene on SAMs

J. Phys. Chem. C, Vol. 114, No. 47, 2010 **20123**

Figure 3. Maximum island density as a function of submonolayer growth rate for the deposition of PFP on SiO_2 and SiO_2 terminated with four different self-assembled MLs. In all cases, the incident kinetic energy was $E_i = 4.6$ eV, and the substrate temperature was $T_s = 40$ °C. The straight lines represent a fit to a power law. The inset shows the critical island size, i^*, as a function of surface termination.

Figure 4. Atomic force micrographs, 3×3 μm^2, of submonolayer thin films of PFP grown on five different surfaces: (d) SiO_2 (0.24 ML of PFP) and SiO_2 terminated with (a) FOTS (0.56 ML), (b) HMDS (0.42 ML), (c) OTS (0.39 ML), and (e) MAOPTS (0.33 ML). The micrographs are in order of decreasing island density, a–e. In panel f, we present an AF micrograph of a PFP film deposited on a SiO_2 surface, representing a thickness of 3.61 ML. In all cases, the incident kinetic energy was $E_i = 4.6$ eV, and the substrate temperature was $T_s = 40$ °C.

Unlike the slopes of the curves shown in Figure 3, at a comparable growth rate, the maximum island density of PFP depends strongly on the nature of the substrate. In particular, the maximum island density of PFP is greatest on FOTS, followed by HMDS, OTS, SiO_2, and MAOPTS. Because $N_x \propto (GR/D)^{i^*/(i^*+2)}$, and because we observed essentially the same value for i^* on all five surfaces, this suggests that the diffusivity, D, of PFP differs on the five surfaces and is mostly responsible for the offsets. An underlying assumption concerning this conclusion is that the prefactor η in eq 1 does not contribute significantly to the observed changes in N_x. For the range of coverages that we consider here ($\theta \sim 0.1–0.4$ ML) and the values for the size of the critical cluster ($i^* \sim 2–4$), we estimate $\eta(\theta, i^*)$ to lie in range 0.2–0.3 for PFP on all surfaces investigated.[37] This difference (less than a factor of 2) clearly does not account for the change in N_x that we observe. Thus, we are left with an explanation that the change in N_x observed has to be the result of a change in the diffusivity, D, of PFP on each surface.

The relative diffusivity of PFP can be estimated by taking the ratio of N_x on any two surfaces at a constant GR (0.005 ML s^{-1}) and using the relationship, $D_2 = D_1[(N_{x,1}/N_{x,2})^{((i^*+2)/i^*)}]$. If we let $D_1 = D_{FOTS} = 1$ and assume $i^* = 2.66$ (vide supra), then by implication, $D_{HMDS} = 7.1$, $D_{OTS} = 35$, $D_{SiO_2} = 67$, and $D_{MAOPTS} = 115$. *This analysis suggests that the diffusivity of PFP is a strong function of the chemical and structural nature of the underlying substrate.* Other work has found differences in island densities with surface termination—in particular, concerning growth of pentacene on SiO_2 vs Si(100) surfaces terminated with H[40] or cyclohexene.[15] In these studies, the island densities were highest on a chemically oxidized SiO_2 surface[40] and a plasma-cleaned and annealed thin SiO_2 gate oxide.[15]

The thin films of PFP have also been characterized using grazing incidence diffraction (GID) at the CHESS G2 station to verify the in-plane crystalline structure and to examine the possibility if the structure was sensitive to the underlying layer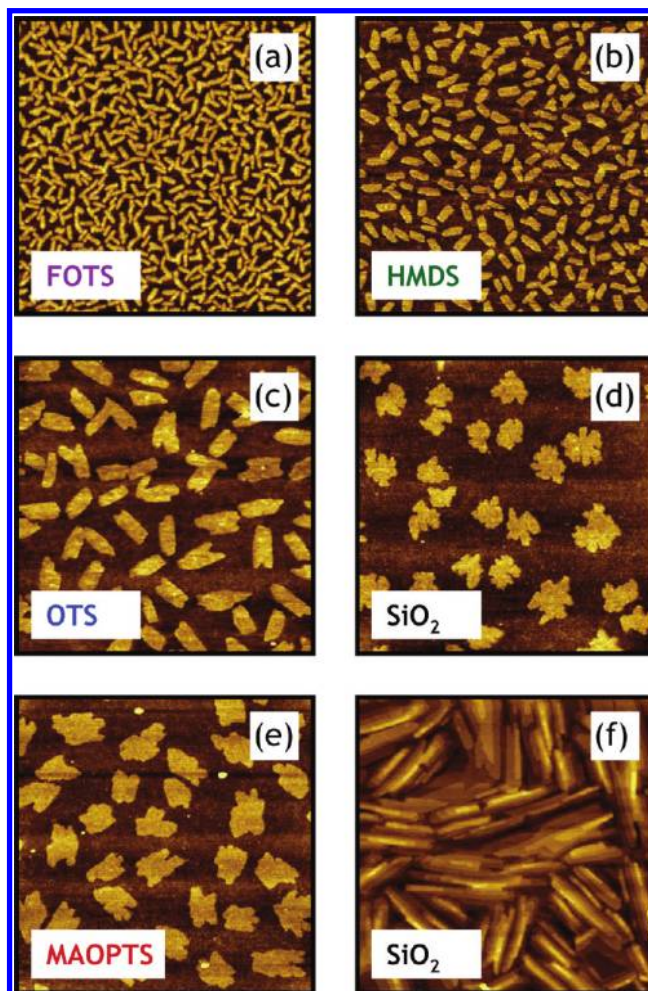. Ex situ analysis using GID on ~4 ML thick PFP films on all surfaces showed essentially no differences in the positions of the in-plane reflection planes, and the positions of the peaks were consistent with earlier reports.[33,35] Ex situ analysis using GID on thinner ~1.5 ML PFP films showed only minor differences in the positions of the (120) and (130) reflection planes (the most intense observed here) on all surfaces. For example, from previous work, $q_{(120)} = 1.771$[33] and 1.772 Å^{-1},[35] whereas we found values ranging from 1.762 to 1.773 Å^{-1}. Likewise, in previous work, $q_{(130)} = 2.158$[33] and 2.153 Å^{-1},[35] whereas we found values ranging from 2.149 to 2.168 Å^{-1}. These values represent a difference of at most 0.6–0.7%. We do not believe such small changes in the crystal structure in the ML regime are significant enough to explain other observations that we make here concerning phenomena that show a dependence on surface termination.

The nature of the SAM not only affects the island density of PFP but also the submonolayer island shapes. In Figure 4, we display representative AF micrographs of PFP in the submonolayer regime for growth on all of the surfaces examined here. The corresponding coverages and GRs for these films are all within a factor of ~2 and are given in the figure. On FOTS, HMDS, and OTS, the PFP islands are anisotropic with a
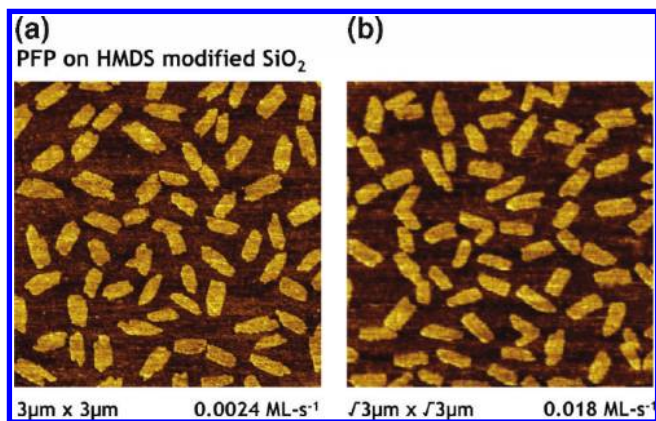
Figure 5. Atomic force micrographs of submonolayer thin films of PFP grown on a SiO$_2$ surface terminated with HMDS at rates of (a) 0.00240 and (b) 0.0180 ML s^{-1}. As presented, the scale in (a) is 3 × 3 μm^2, while that in (b) is 3$^{1/3}$ × 3$^{1/3}$ μm^2. The axes have been scaled to produce what appear to be equivalent island densities to highlight the similarities in island shapes. In all cases, the incident kinetic energy was E_i = 4.6 eV, and the substrate temperature was T_s = 40 °C.

compact polygonal shape. The aspect ratio of these islands is approximately ∼2−4, and it is greater on FOTS as compared to HMDS and OTS. In contrast, the islands on MAOPTS and SiO$_2$ are clearly not compact polygons and are much more irregular. The shapes of these islands are similar to those reported for growth of pentacene on SiO$_2$[13,15,40] but are not nearly as fractal as those reported for pentacene on H- and cyclohexene-terminated Si(100).[15,40]

We note that the changes that we observe in island shape with surface termination do not depend on the growth rate for each surface examined. To examine this explicitly, we consider again the results that we presented in Figure 2 concerning the growth of PFP on HMDS. In Figure 5, we present micrographs representing the lowest and highest growth rate examined, where we have scaled the images such that the apparent island density (number of islands in the image) is constant, even while the growth rate changes from 2.4 × 10^{-3} to 18.0 × 10^{-3} ML s^{-1} or a factor of 7.5. As may be seen, the shapes and aspect ratios of the islands for the two extremes of growth rates examined are essentially indistinguishable from each other. Thus, it is clear that the change in the rate of growth cannot explain the change in the island shape and that the differences observed in submonolayer island shapes are most strongly influenced by the substrate−PFP interactions.

Unlike the features formed in the submonolayer regime, once the substrate is covered, the morphologies of the PFP thin films in the multilayer regime are all remarkably similar. A representative micrograph is shown in Figure 4f for the case of a ∼4 ML thick film on SiO$_2$. As may be seen, the features in this coverage regime are very anisotropic and are narrow and rodlike, similar to what has been reported previously.[32,33] As expected for growth on substrates lacking crystallographic order, we see that different grains are evidently randomly oriented with respect to each other and to the substrate. However, there is some short-range order as small "bundles" of these rodlike features are observed. It is interesting to note that the submonolayer islands that most resemble these features observed in the multilayer regime are those formed on FOTS.

The shape of islands in the submonolayer regime can be the consequence of both energetic (thermodynamic) and kinetic factors. Not unlike the situation concerning the 3D evolution of surface morphology and roughness, similar molecular scale events contribute to the structures that are formed in 2D. There

are important differences, however, between these essentially 2D and 3D phenomena. Our results indicate that the diffusivity of PFP varies greatly on the five surfaces examined here, by as much as 2 orders of magnitude. We expect that diffusion of PFP on these starting substrates involves the molecule laying flat (to maximize van der Waals interactions), assuming that the underlying SAM is sufficiently dense such that PFP is unlikely to penetrate the organic ML. In contrast, the molecules that are part of both the growing islands and the multilayer thin film are standing up, with their long molecular axis nearly perpendicular to the surface. Thus, the interaction with the underlying substrate is expected to be fundamentally different concerning diffusing admolecules vs molecules incorporated into the crystals. Thus, fast diffusion on a substrate need not translate into fast diffusion around the periphery of an island or vice versa.

In terms of molecular scale events that occur as islands grow and begin to adopt a shape, the first event has to involve attachment of a molecule to the island edge. At low coverages and assuming adsorption is irreversible on the substrate surface, prior to attachment, these molecules will adsorb first on the bare substrate and then diffuse to the island edge (as compared to adsorbing on top of the island and diffusing to the island edge). Given the shape of these molecules and the nature of the molecule−substrate and molecule−molecule interactions (essentially van der Waals), there could be a barrier to the attachment process, as the molecule must reorient itself with respect to binding flat on the substrate surface to binding nominally upright at the island edge (vide infra). Some sort of sliding or flipping motion would seem to be necessary, which may be facilitated by nearby molecules either in the island or representing the underlying SAM. We note that such motions involving reorientation do not occur in atomic (epitaxial) systems such as Pt on Pt(111), where island shapes have been the focus of several investigations,[41] as they are properly modeled as particles with spherical symmetry. The final state—a molecule bound to an island edge—is expected to depend on the local structure, for example, which crystal face is exposed at the island edge. In extreme cases, one might imagine that molecules diffusing on a particular substrate and impacting a particular crystal face of an island edge may be reflected, whereas some other combination could lead to very efficient incorporation/attachment. Such "anisotropic sticking" or "anisotropic accommodation", as suggested in work on atomic epitaxial systems,[41,42] could explain the formation of anisotropic islands, which has been suggested to occur in other small molecule organic systems.[43]

Island shape can also be determined by energetic/thermodynamic factors. Given differences in the surface energy of different crystallographic orientations, an island may seek to minimize high energy edges vs low energy ones. Such a process would depend on the fast diffusion of molecules around the edges of islands, including corners where added barriers to diffusion may exist. In 3D, diffusion of atoms from one terrace to another is hampered by the well-known step-edge, or Ehrlich−Schwoebel, barrier.[44,45] Such a barrier also exists in molecular systems,[46−48] which we examine here. In 2D, an analogous "island corner crossing" barrier has been identified concerning atomistic epitaxial growth.[49] Undoubtedly, a similar barrier exists for molecular systems. If energetic factors are determining island shapes and we are below a temperature where entropy-driven island edge roughening is important, then one would expect compact islands, with possibly relatively straight

Nucleation and Growth of Perfluoropentacene on SAMs

J. Phys. Chem. C, Vol. 114, No. 47, 2010 **20125**

edges. Such seems to be the case for the islands on FOTS, HMDS, and OTS, not so for the islands formed on MAOPTS and SiO$_2$.

Reviewing our results as a whole concerning island shape, we consider some potential scenarios. First, can the islands formed here restructure/reorganize during growth and hence influence the shapes that are formed? One test of the extent of postdeposition island shape evolution is to examine what occurs under extended aging. For example, concerning near-ML coverages of pentacene on FOTS and HMDS, we have found that these films undergo significant postdeposition reorganization if left under vacuum for a period of time ranging from a few minutes (on FOTS) to ~120 min (on HMDS).[16] To test this possibility here, we compared AF micrographs for samples of PFP on SiO$_2$ and FOTS where in each case samples were removed almost immediately after growth (~2 min) or were left under vacuum for ca. 150 min. The images for these submonolayer films (not shown here) were essentially indistinguishable in terms of both island shape and density. Additional aging in air for ~2 months also did not produce any changes in island shape and density. Thus, either the films formed here do not reorganize or they do on a time scale that is short with respect to the time it takes to remove a sample from vacuum (<2 min). We note this latter time period is not so different from the time of growth (~0.4−0.7 min for Figure 4a−e). Indeed, reviewing the results from Figure 5, where the total time of growth varied from 0.4 to 2.5 min, we do not observe any noticeable changes in island shape, even while the density is changing by a factor of ~3.

On the basis of the previous discussion, we are left with a picture where either reorganization does not occur, or it is very fast as compared to the time scale of the experiments (≪ min). We can argue against the latter interpretation using the following argument. If reorganization is fast, then it is on both SiO$_2$ and FOTS for the conditions examined here, as both terminations showed no effects during postdeposition aging. In this case, we would be left with the unusual situation where reorganization leads to different island shapes depending on the underlying substrate, also while the densities of these islands are changing. We believe this to be unlikely; thus, we are left with the conclusion that other factors are contributing to the island shapes.

Island shape can be influenced by the kinetics of admolecule attachment. As described above, the molecular motions associated with attachment of a molecule at an island edge can be quite complex and may involve contributions of molecules present in the underlying layer. We note that this is quite unlike atomistic epitaxial growth, as indicated above, and a simple comparison is displayed in schematic form in the upper panel of Figure 6. Indeed, as discussed above, it is actually likely that a barrier exists to admolecule attachment as the molecule reorients from lying down to standing up. Once attached, the molecule may diffuse around the periphery of an island before finding a preferred binding site, exhibiting a form of transient mobility. We would distinguish such a process from large-scale reorganization if the final step of binding to a preferred site is effectively irreversible.

How might the bonding of PFP vary from site to site on an island edge? If we use pentacene as a guide, calculations using DFT-LDA indicate that the binding of pentacene varies significantly concerning the likely low index crystalline facets present on the edges of the islands.[50] For example, pentacene is bound by ~0.9 eV on the relatively smooth (100) face, ~0.75 eV on the (110) and (1$\bar{1}$0) faces, and ~1.2 eV on the (010)
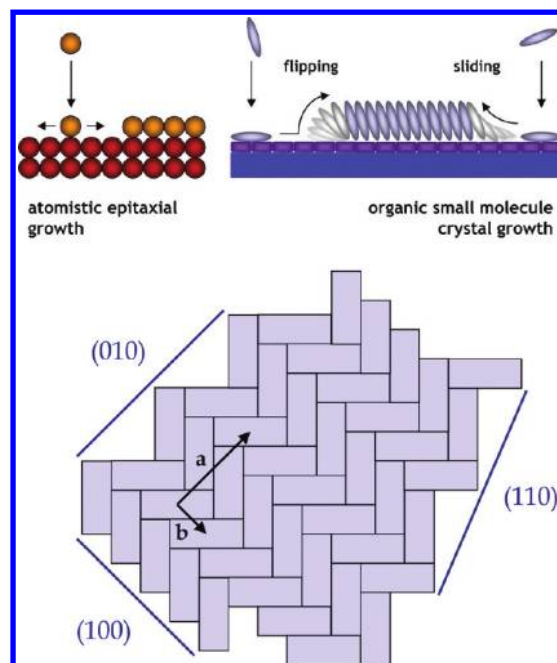

Figure 6. Upper panel: Schematic representation of the motions associated with adatom attachment to a submonolayer island and admolecule attachment to a submonolayer island, where these molecules are "standing upright". Lower panel: A simple model for the shape of an island of PFP formed in the submonolayer regime, based on the known crystal structure, where the surface exposed is the (001) plane. We assume here that the herringbone angle is exactly 90°, where a PFP molecule can be represented in-plane by a rectangle. The two in-plane lattice vectors are shown, a = 11.4 Å, and b = 4.5 Å.

face. More recent calculations of this same system using a density functional that better describes van der Waals interactions suggest that these energies may be underestimated by 25−50%.[51] Using these results, the binding of pentacene to the (100), (110), and (010) faces may be closer to 1.25, 1.13, and 1.52 eV. At room temperature, using these binding energies, the difference in residence time between the (100) and (010) faces could be on the order of $4 \times 10^4 - 1 \times 10^5$. In this scenario, the (010) faces could act effectively as sinks, and growth could preferentially proceed in this direction.

In terms of equilibrium shapes, we are aware of no studies of PFP concerning this issue. There are examinations of pentacene, however. Concerning pentacene, calculations indicate that islands should be approximately hexagonal in shape, consisting of (100), (110), and (1$\bar{1}$0) edges and either devoid of (010) edges[50] or possessing small facets presenting this face.[51] No study predicts the presence of square corners in the equilibrium crystal shape produced by the intersection of (100) and (010) faces. Examining the images given in Figures 2, 4, and 5, we observe a variety of acute, obtuse, and, without question, some right angles, especially on HMDS and OTS. How might these images be related to PFP equilibrium crystal shapes? To answer this question, we now consider what is known about the crystal structure of PFP.

The structure of PFP is similar to that of pentacene, but there are important differences. For example, the angle between neighboring molecules in the herringbone rows is nearly 90° (91.2°) for PFP vs 51.9° for pentacene.[34] Using what is known about the size and shape of the unit cell of PFP,[34] we can construct a simple model for the shape of the PFP islands in the submonolayer regime. In particular, the in-plane lattice constants are given by a = 11.40−11.48 Å, b = 4.49−4.53 Å, and γ = 90°.[33−35] In the lower panel of Figure 6, we consider

a simple model for the packing of PFP molecules in the unit cell, where we assume that the herringbone angle is exactly 90°. In this case, the in-plane space occupied by each PFP molecule can be approximated by a rectangle, where the aspect ratio is determined by the ratio of lattice constants $b/a \sim 0.39$.[34] On the basis of this simple construction, similar to what has been applied to the case of pentacene,[50] the (100) face can be expected to be a low surface energy face. The other low index face, the (010), although exhibiting more molecular scale roughness as shown in Figure 6, might also be expected to be a low surface energy face. Perhaps of most interest here, the (110) face would appear to be almost degenerate in surface energy with the (010) face.

If we assume that the islands formed possess a number of edges that represent the low index (100), (110), and (010) faces, then a quantitative analysis of the island shapes would seem to be in order. Unlike the analysis of 3D topology, analysis of 2D shapes formed in the submonolayer regime is not widely reported, and there are no standard or well-established methods that are commonly employed (outside of fields such as cartography). We make use of two methods here, which are by no means unique. We will also only report the results for the analyses on FOTS, HMDS, and SiO₂. The results for OTS are quite similar to those on HMDS, while the same is true for MAOPTS and SiO₂. First, we used MATLAB to produce a topological map of the submonolayer structures. By selecting the appropriate "height", the islands become a series of closed curves. Islands not making closed curves, for example, those at the edge of the micrographs, were not included in the analyses. Next, given these curves, we then applied the Douglas–Peucker algorithm[52,53] to find "best fit" polygons for each island. Here, the analysis was somewhat subjective, as depending on the size of the tolerance parameter used in the fit, the algorithm can fit a shape to a very large number of vertices giving an uninformative and, perhaps, unphysical representation of the island shape. For example, for the relatively compact islands observed on FOTS, HMDS, and OTS, one expects to limit the number of vertices to fewer than those for the islands on MAOPTS and SiO₂.

In Figures 7 and 8, we present the results of our analysis of the island shapes. To clearly illustrate our method in Figure 7, we consider only the analysis of single islands formed on HMDS and SiO₂. The first row includes the shapes found by applying the Douglas–Peucker algorithm, and the longest edge is highlighted by a dotted line in each case. In the second row, we plot the (unweighted) histograms for the vertex angles and, as may be seen the island on SiO₂, gives both convex and concave vertices. In the third row, we consider another representation of the island shapes. Here, we consider the angles that the faces make with each other, regardless if the facets meet to make a corner. In this analysis, the longest side of each polygon defines 0°, and the edges are treated as vectors such that the possible angles range from 0° to 360°. In this construction, we also weight the distribution by the length of the edge. For HMDS, the long, nearly parallel faces produce a peak in the distribution, whereas on SiO₂ the distribution is much broader.

In Figure 8, we present a full analysis of the islands formed on FOTS, HMDS, and SiO₂, where in the top row we present micrographs for films deposited at rates of 0.0021, 0.0056, and 0.0019 ML s⁻¹, representing coverages of 0.119, 0.361, and 0.388 MLs, respectively. In the second row, we present the shapes that were fit to each of the islands analyzed. The number of islands analyzed were 135, 74, and 131 for PFP on FOTS,
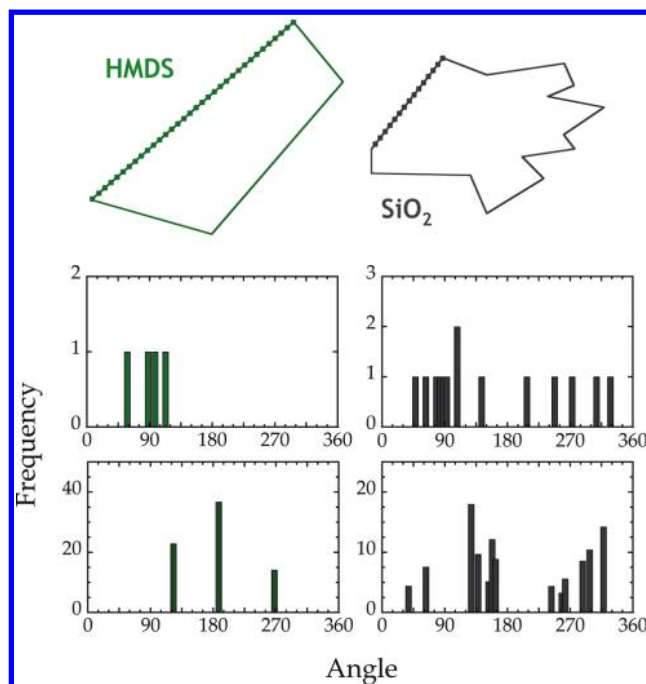

Figure 7. Illustrative figure demonstrating the method that we use to analyze island shapes. First row: shapes of single islands found from an analysis of the atomic force micrographs of PFP on HMDS and SiO₂. Second row: histograms of the vertex angles represented by the polygons. Third row: histograms of the angles of relative orientation between the sides of the polygons, with respect to the longest edge, and weighted to the length of the edge.

HMDS, and SiO₂, respectively. Here, for the number of vertices, our analysis gave these values (means and standard deviations): 4.70 ± 1.17, 5.70 ± 2.28, and 14.61 ± 6.58 for PFP on FOTS, HDMS, and SiO₂, respectively. As may be appreciated, the shapes have been well captured by this analysis. In the third row, we plot histograms of the unweighted population of vertex angles in the fitted polygons. Here, we see an obvious difference for the results on FOTS and HMDS vs that on SiO₂. As the former two surfaces are populated mostly by compact islands, these histograms are described by a single Gaussian distribution. For FOTS, we find that the mean is $\sim 99°$, with a standard deviation of 33°, while for HMDS, we find 104° and 37°, respectively. On SiO₂, we see that the distribution is bimodal, because of the noncompact shapes, and that two Gaussians fit the data: $103 \pm 27°$ and $264 \pm 38°$. If the low index faces dominate the populations, we would expect peaks in the distribution (for angles <180°) at angles of 43, 69, 90, 111, and 137° (cf. Figure 6). These values are certainly represented in all cases examined here, but we hesitate to make a stronger conclusion at this point in the analysis.

In the fourth row of Figure 8, we plot the histograms of the relative angles between edges of the fitted polygons and the longest edge, applying a weighting factor given by the length of the edge, as we described in connection with Figure 7. Again, we take note of important differences concerning the results for FOTS, HMDS, and SiO₂. First, the distribution on FOTS is highly peaked at an angle of $\sim 180°$. Indeed, the two bins representing angles from 175 to 185° represent 39% of this length-weighted histogram, while a fit to a Gaussian gives a mean and standard deviation of $180.7 \pm 3.5°$. This means that on FOTS there is a strong tendency for the formation of islands possessing parallel facets or edges. Given the structure discussed above in connection with Figure 6, it seems likely that these would be the (100) and ($\bar{1}$00) faces. There is also a hint of higher
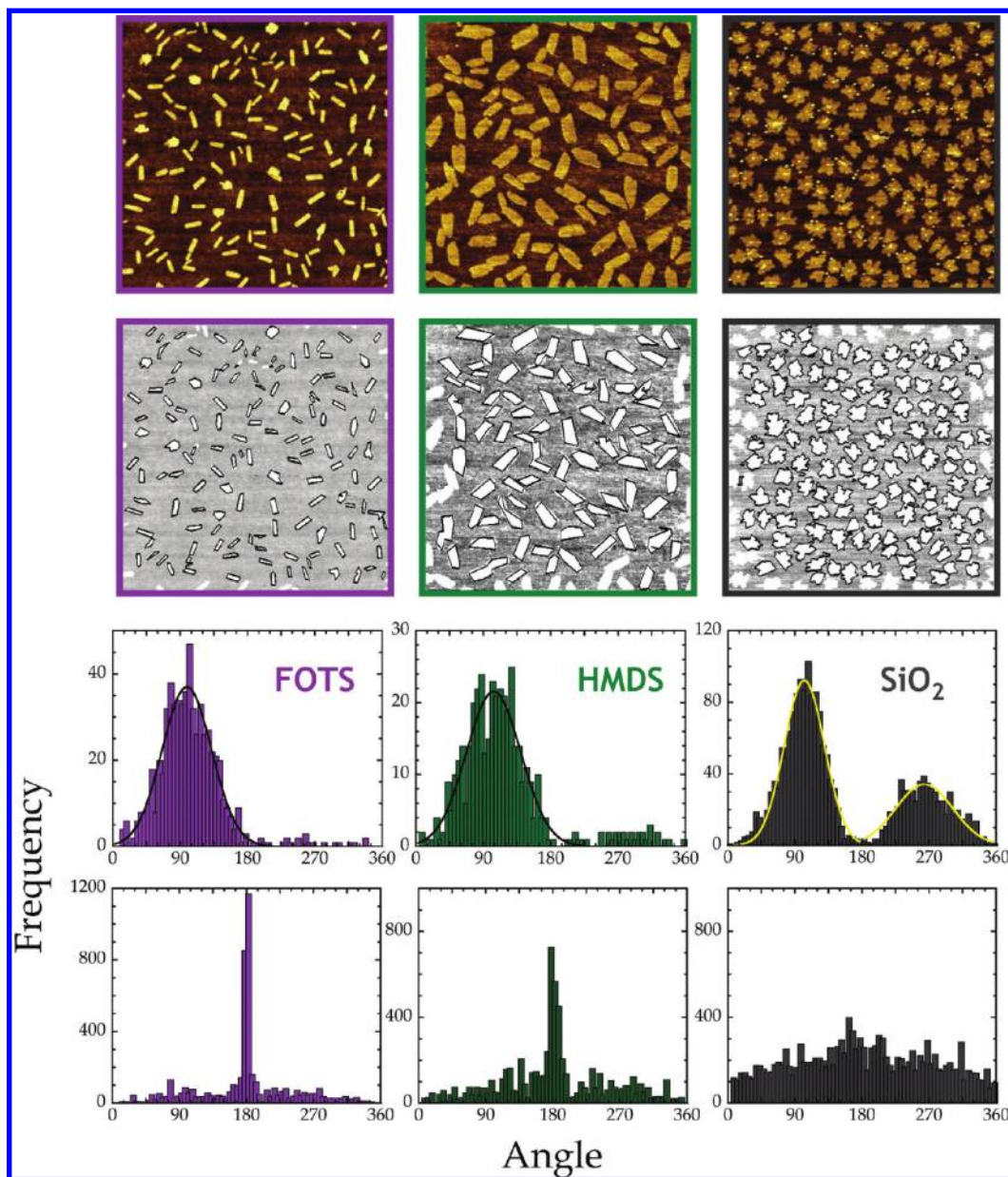
Figure 8. First row: Atomic force micrographs of submonolayer thin films of PFP grown on (left to right) FOTS, HMDS, and SiO$_2$. The first two of these images are 3×3 μm^2, and the latter is 10×10 μm^2. Second row: Analysis of island shapes as simple polygons using the approach described in the text. Third row: Histograms of the vertex angles represented by the polygons. Fourth row: Histograms of the angles of relative orientation between the sides of the polygons, with respect to the longest edge, and weighted to the length of the edge.

frequencies for angles of ∼80−100°, but a peak in this range is much less obvious. On HMDS, the histogram is similar to that on FOTS but not as peaked at an angle of ∼180°. Here, the four bins representing angles from 170 to 190° represent 29% of this length-weighted histogram, while a fit to a Gaussian gives a mean and standard deviation of 181.0 ± 7.9°. Thus, this surface also tends to form islands that possess parallel edges, but the larger contribution of edges not close to 180°, as compared to FOTS, indicates that the aspect ratios of the islands are smaller on this surface. Finally, on SiO$_2$, the edge-length weighted distribution is very broad and does not exhibit an obvious peak. A fit of these data to a Gaussian gives a mean and standard deviation of 180 ± 137°. These results are consistent with the noncompact nature of the islands that are formed on SiO$_2$.

Summing up the results of our analysis displayed in Figure 8 concerning the shapes of the islands, we find that the largely objective analysis described above mostly verifies what is seen

by the naked eye. First, the islands on FOTS and HMDS (and OTS, cf. Figure 4) are compact, and ∼70% of the vertex angles lie within a range of 65−140°, with the distribution peaking near 100°. These results are consistent with the existence of corners produced by the intersection of (100) edges with both (110) and (010) edges. The large predominance of parallel edges, particularly on FOTS, but less dominant on HMDS (and OTS), strongly suggests that many islands possess long (100) and ($\bar{1}$00) faces as edges. These parallel edges are also quite noticeable for multilayer films of PFP on all surfaces, cf. Figure 4f. On SiO$_2$ (and MAOPTS), the islands are not compact and a number of vertex angles lie in the range of 180−360°. Also, on these surfaces, there is only a very weak tendency to form islands with parallel edges.

In concluding our discussion of island shape variation with surface termination, we make the following observation. Although it is likely that equilibrium shapes are not achieved on any surface, there is a connection between equilibrium concepts

and those based on molecular events such as admolecule attachment, diffusion along edges and across corners, and preferential binding. Low energy edges, such as the (100), will bind admolecules weakly and tend to "donate" these molecules to bind at higher energy edges such as the (010) and the (110). Thus, if corner crossing is facile, then one can imagine the formation of islands with straight parallel (100) edges. Large barriers to island corner crossing, however, will tend to lead to instabilities in the evolution of island shape, and islands that are not compact will tend to form.[49] If barriers to island corner crossing are playing a role in the islands that are formed on SiO₂ and MAOPTS, then these barriers are apparently much different for PFP on FOTS, HMDS, and OTS. As the short edge of PFP interacts most directly with the underlying substrate, this sensitivity is unexpected. This is particularly curious as the mobility of flat lying, isolated PFP molecules is highest on the MAOPTS and SiO₂ surfaces.

IV. Conclusions

In conclusion, we have examined the nucleation and growth of PFP on a series of surfaces represented by differing chemical terminations and surface energies. PFP was chosen because of its low intrinsic surface energy—we do not expect it to dewet or reorganize on low energy surfaces. This enabled us to study the effect of SAMs on the nucleation and growth of a crystalline organic thin film, which is otherwise very problematic to examine. On all surfaces examined, PFP forms single molecule-high islands in the submonolayer regime, which are stable in density, shape, and size with extended aging. Furthermore, PFP exhibits the characteristics of homogeneous nucleation on all surfaces. We found that the chemical structure of the SAM significantly affects the nucleation density of PFP under otherwise identical conditions of growth. In particular, the density of islands on FOTS (the lowest surface energy SAM examined) exceeded that on MAOPTS (the highest surface energy SAM examined) by over an order of magnitude. At the same time, the size of the critical nucleus indicated by the change in island density with growth rate showed no dependence on surface termination, and a value of $i* \sim 2-3$ could describe all data. We are left to conclude that the change in island density is due to a change in the diffusivity of PFP admolecules on these surfaces by as much as 2 orders of magnitude. The chemical structure of the SAM also significantly affects the shapes of the islands of PFP formed in the submonolayer regime. Interestingly, the islands are most compact and faceted on those surfaces where diffusion of isolated PFP admolecules is indicated to be the slowest. The shapes of the islands formed on all surfaces were analyzed in terms of simple polygonal shapes. These shapes were consistent with the islands possessing a number of the low index edges, that is, the (100), (010), and (110), including parallel (100) edges on surfaces terminated by FOTS, HMDS, and OTS. Our observations suggest that the molecular motions and intermolecular interactions describing the diffusion of isolated admolecules are quite different from those concerning molecules moving on the periphery of a growing island. Finally, once the substrate surface is covered, the growth becomes very 3D on all surfaces, and a rough multilayer morphology is observed. For these thick films, very anisotropic features are formed, which may suggest the predominance of a single face at these coverages, such as the (100) orientation.

References and Notes

(1) Hamers, R. J. *Nature* **2001**, *412*, 489–490.
(2) Dimitrakopoulos, C. D.; Malenfant, P. R. L. *Adv. Mater.* **2002**, *14*, 99–117.
(3) Lin, Y. Y.; Gundlach, D. J.; Nelson, S. F.; Jackson, T. N. *IEEE Electron Device Lett.* **1997**, *18*, 606–608.
(4) Ruiz, R.; Papadimitratos, A.; Mayer, A. C.; Malliaras, G. G. *Adv. Mater.* **2005**, *17*, 1795–1798.
(5) Dinelli, F.; Murgia, M.; Levy, P.; Cavallini, M.; Biscarini, F.; de Leeuw Dago, M. *Phys. Rev. Lett.* **2004**, *92*, 116802–116804.
(6) Muck, T.; Wagner, V.; Bass, U.; Leufgen, M.; Geurts, J.; Molenkamp, L. W. *Synth. Met.* **2004**, *146*, 317–320.
(7) Dodabalapur, A.; Torsi, L.; Katz, H. E. *Science* **1995**, *268*, 270–271.
(8) Kelley, T. W.; Boardman, L. D.; Dunbar, T. D.; Muyres, D. V.; Pellerite, M. J.; Smith, T. P. *J. Phys. Chem. B* **2003**, *107*, 5877–5881.
(9) Yang, H.; Shin, T. J.; Ling, M. M.; Cho, K.; Ryu, C. Y.; Bao, Z. *J. Am. Chem. Soc.* **2005**, *127*, 11542–11543.
(10) Virkar, A.; Mannsfield, S.; Oh, J. H.; Toney, M. F.; Tan, Y. H.; Liu, G.; Scott, J. C.; Miller, R.; Bao, Z. *Adv. Funct. Mater.* **2009**, *19*, 1962–1970.
(11) Shtein, M.; Mapel, J.; Benziger, J. B.; Forrest, S. R. *Appl. Phys. Lett.* **2002**, *81*, 268–270.
(12) Klauk, H.; Halik, M.; Zschieschang, U.; Schmid, G.; Radlik, W.; Weber, W. *J. Appl. Phys.* **2002**, *92*, 5259–5263.
(13) Killampalli, A. S.; Schroeder, T. W.; Engstrom, J. R. *Appl. Phys. Lett.* **2005**, *87*, 033110/1−033110/3.
(14) Ruiz, R.; Nickel, B.; Koch, N.; Feldman, L. C.; Haglund, R. F., Jr.; Kahn, A.; Family, F.; Scoles, G. *Phys. Rev. Lett.* **2003**, *91*, 136102/1–136102/4.
(15) Meyer zu Heringdorf, F.-J.; Reuter, M. C.; Tromp, R. M. *Appl. Phys. A: Mater. Sci. Process.* **2004**, *78*, 787–791.
(16) Amassian, A.; Pozdin, V.; Desai, T. V.; Hong, S.; Woll, A. R.; Ferguson, J. D.; Brock, J. D.; Malliaras, G. G.; Engstrom, J. R. *J. Mater. Chem.* **2009**, *19*, 5580–5592.
(17) Burke, S. A.; Topple, J. M.; Grütter, P. *J. Phys: Condens. Mater.* **2009**, *21*, 423101/1–423101/16.
(18) Schroeder, T. W. Ph.D. Thesis; Cornell University, 2004.
(19) Hong, S.; Amassian, A.; Woll, A. R.; Bhargava, S.; Ferguson, J. D.; Malliaras, G. G.; Brock, J. D.; Engstrom, J. R. *Appl. Phys. Lett.* **2008**, *92*, 253304/1–253304/3.
(20) Krause, B.; Schreiber, F.; Dosch, H.; Pimpinelli, A.; Seeck, O. H. *Europhys. Lett.* **2004**, *65*, 372–378.
(21) Schreiber, F. *Prog. Surf. Sci.* **2000**, *65*, 151–256.
(22) Kaelble, D. H. *J. Appl. Polym. Sci.* **1974**, *18*, 1869–1889.
(23) Knieling, T.; Lang, W.; Bencke, W. *Sens. Actuators, B* **2007**, *126*, 13–17.
(24) Kawai, A.; Kawakami, J. *J. Photopolym. Sci. Technol.* **2003**, *16*, 665–668.
(25) Braun, C. *Parratt32 Program*; Berlin Neutron Scattering Center (BENSC): Hahn-Meitner Institut, 1997.
(26) Tolan, M. *X-ray Scattering from Soft-Matter Thin Films*; Springer: Berlin, 1999.
(27) Killampalli, A. S.; Engstrom, J. R. *Appl. Phys. Lett.* **2006**, *88*, 143125/1–143125/3.
(28) Amassian, A.; Desai, T. V.; Kowarik, S.; Hong, S.; Woll, A. R.; Malliaras, G. G.; Schreiber, F.; Engstrom, J. R. *J. Chem. Phys.* **2009**, *130*, 124701/1–124701/9.
(29) Kowarik, S.; Gerlach, A.; Skoda, M.; Sellner, S.; Schreiber, F. *Eur. Phys. J. Spec. Top.* **2009**, *168*, 11–18.
(30) Woll, A. R.; Desai, T. V.; Engstrom, J. R. Manuscript in preparation.
(31) Cohen, P. I.; Petrich, G. S.; Pukite, P. R.; Whaley, G. J.; Arrott, A. S. *Surf. Sci.* **1989**, *216*, 222–248.
(32) Hinderhofer, A.; Heinemeyer, U.; Gerlach, A.; Kowarik, S.; Jacobs, R. M. J.; Sakamoto, Y.; Suzuki, T.; Schreiber, F. *J. Chem. Phys.* **2007**, *127*, 194705/1–194705/6.
(33) Kowarik, S.; Gerlach, A.; Hinderhofer, A.; Milita, S.; Borgatti, F.; Zontone, F.; Suzuki, T.; Biscarini, F.; Schreiber, F. *Phys. Status Solidi* **2008**, *2*, 120–122.
(34) Sakamoto, Y.; Suzuki, T.; Kobayashi, M.; Gao, Y.; Fukai, Y.; Inoue, Y.; Sato, F.; Tokito, S. *J. Am. Chem. Soc.* **2004**, *126*, 8138–8140.
(35) Salzmann, I.; Duhm, S.; Heimel, G.; Rabe, J. P.; Koch, N.; Oehzelt, M.; Sakamoto, Y.; Suzuki, T. *Langmuir* **2008**, *24*, 7294–7298.
(36) Venables, J. A. *Phys. Rev. B* **1987**, *36*, 4153–4162.
(37) Venables, J. A.; Spiller, G. D. T.; Hanbücken, M. *Rep. Prog. Phys.* **1984**, *47*, 399–459.

Nucleation and Growth of Perfluoropentacene on SAMs

J. Phys. Chem. C, Vol. 114, No. 47, 2010 **20129**

(38) Zhang, Z.; Lagally, M. G. *Science* **1997**, *276*, 377–383.

(39) Brune, H. *Surf. Sci. Rep.* **1998**, *31*, 121–229.

(40) Ruiz, R.; Nickel, B.; Koch, N.; Feldman, L. C.; Haglund, R. F.; Kahn, A.; Scoles, G. *Phys. Rev. B* **2003**, *67*, 125406/1–125406/7.

(41) Michely, T.; Hohage, M.; Bott, M.; Comsa, G. *Phys. Rev. Lett.* **1993**, *70*, 3943–3946.

(42) Mo, Y.-W.; Swartzentruber, B. S.; Kariotis, R.; Webb, M. B.; Lagally, M. G. *Phys. Rev. Lett.* **1989**, *63*, 2393–2396.

(43) de Oteyza, D. G.; Barrena, E.; Sellner, S.; Ossó, J. O.; Dosch, H. *J. Phys. Chem. B* **2006**, *110*, 16618–16623.

(44) Ehrlich, G.; Hudda, F. G. *J. Chem. Phys.* **1966**, *44*, 1039–1049.

(45) Schwoebel, R. L.; Shipsey, E. J. *J. Appl. Phys.* **1966**, *37*, 3682–3686.

(46) Fendrich, M.; Krug, J. *Phys. Rev. B* **2007**, *76*, 121302/1–121302/3.

(47) Hlawacek, G.; Puschnig, P.; Frank, P.; Winkler, A.; Ambrosch-Draxl, C.; Teichert, C. *Science* **2008**, *321*, 108–111.

(48) Goose, J. E.; First, E. L.; Clancy, P. *Phys. Rev. B* **2010**, *81*, 205310/1–205310/20.

(49) Zhong, J.; Zhang, T.; Zhang, Z.; Lagally, M. G. *Phys. Rev. B* **2001**, *63*, 113403/1–113403/4.

(50) Northrup, J. E.; Tiago, M. L.; Louie, S. G. *Phys Rev. B* **2002**, *66*, 121404/1–121404/4.

(51) Nabok, D.; Puschnig, P.; Ambrosch-Draxl, C. *Phys. Rev. B* **2008**, *77*, 245316/1–245316/4.

(52) Ramer, U. *Comput. Graphics Image Process.* **1972**, *1*, 244–256.

(53) Douglas, D. H.; Peucker, T. K. *Can. Cartographer* **1973**, *10*, 112–122.